Modeling and Analysis of the Bendable Transformer

Godwin Kwun Yuan Ho, *Student Member, IEEE*, Cheng Zhang, *Student Member, IEEE*, Bryan M. H. Pong, *Senior Member, IEEE*, and S. Y. Ron Hui, *Fellow, IEEE*

***Abstract*—This paper presents a study of a bendable transformer for wearable electronics. Printed on a thin and bendable film, this transformer is bendable to wrap around body limbs such as the forearm. A model using a partial equivalent circuit theory has been developed to analyze the characteristic of an inductor and a bendable transformer. The mutual inductance and self-inductance for the bendable transformer over a range of bent curvatures have been calculated based on the model and compared favorably with measurements. Simulation and experimental results of applying the bendable inductor and transformer in dc–dc converters as a 5-V 500-mA power supply are included to confirm the usefulness of the transformer and the validity of the model.**

***Index Terms*—Buck converter, flexible transformer, *LLC* resonant converter, wearable electronics.**

I. Introduction

WEARABLE electronics products like smart watches, hearing aids, intelligent glasses, are becoming popular nowadays. Wearable electronic products appeared back in 1950s [1]. A good portable electronic product should be small in size and light in weight. A good wearable electronics product needs one more requirement: comfortable to wear. This requirement introduces a new challenge: physically flexible. Many flexible electronics components are available nowadays like flexible display, flexible solar cell, printed RFID, flexible lighting, and others based on the application [2]–[7]. It was estimated that there were about 1500 research units working on flexible electronics in worldwide in 2010 [8]. However, there is a lack of flexible power converter.

A bendable converter can be used in many wearable applications. For example, a bendable converter can be mounted into a jacket with a flexible film solar panel and converts power form solar energy. Another example is to have a bendable converter mounted into a belt fitted with batteries and turns the belt into a central power source for various portable devices. There can be many innovative applications but all will need a fundamental building block which is the bendable converter.

Flexible electronics including passive components are needed for wearable electronics. For switched-mode power supplies, inductor, and transformer are essential passive components. Although non-isolated converter with inductor can fulfill the power conversion requirement of the wearable electronics, isolated converter is also needed for some applications such as medical application.

Traditional magnetic core-based inductor and transformers are not bendable. Although many researchers have worked to improve the thickness, power density, and efficiency of planar transformer, not much work has been done on bendable transformer [8]–[11]. Inductor and coreless printed circuit board (PCB) transformer [12]–[16] is applicable to wearable electronics. It has the advantages of having no core loss, and, thus, being suitable for high-frequency operation. Based on resonant technique, it has been successfully demonstrated in signal and power transfer applications, such as isolated gate drives [12] and planar converters [16]. The coreless PCB transformer technology has the significance of turning the traditional solid transformers into flat ones, making it possible for embedment in power semiconductor integrated circuits as confirmed in its industrial adoptions in isolated gate drive integrated circuits [17], [18]. Therefore, if fabricated on a flexible substrate, coreless PCB transformer offers an attractive solution to bendable electronics. However, not much work has been done on flexible inductor and transformer.

The bendable converter for wearable electronics will closely contact the human body and there is concern whether there is adverse effect form EM radiation form the converter. A lot of works have been done on this issue as the mobile phone today is carried by millions of people already. The equipment is not only in close contact with body but also designed to radiate as a primary function. The ICNIRP [19] has collected extensive work and reported that there is no evidence on major medical effect on the human body for such low radiation. The SAR maximum value of exposure is 4 $W \cdot kg^{-1}$, and the recommended occupational exposure is wind down ten times to 0.44 $W \cdot kg^{-1}$. Even so the radiation produced by a bendable converter of the present power level is unlikely to reach such a value.

The shape of flexible inductor or transformer changes when it is bent. When the structure changes its parameters are also changed. It is important to know how these parameters will be changed and how these parameters will affect the switching converter. Most converter works at high frequency in order to cope with the low inductance in coreless device. Resonant techniques have been incorporated in coreless PCB transformer technology since its inception [14], [15]. The inherent high leakage inductance of the coreless PCB converter can be used as resonant inductance in the *LLC* resonant converter [11], [20]–[22].

This paper presents two steps in the development of bendable coreless PCB transformers. First, in order to study possible parameter changes, a bendable model is developed to study the inductor and transformer under different bending angle. Such model is based on the partial element equivalent circuit (PEEC)

Manuscript received May 27, 2015; revised August 13, 2015; accepted October 29, 2015. Date of publication November 13, 2015; date of current version March 25, 2016. Recommended for publication by Associate Editor J. M. Rivas Davila.

The authors are with the Department of Electrical Engineering, University of Hong Kong, Pokfulam, Hong Kong (e-mail: kyho@eee.hku.hk; guszhang@hku.hk; mhp@eee.hku.hk; ronhui@eee.hku.hk).

Color versions of one or more of the figures in this paper are available online at http://ieeexplore.ieee.org.

Digital Object Identifier 10.1109/TPEL.2015.2500606

method [23]. Second, a bendable inductor is made and its inductance measured. It is then applied to a buck converter. On the other hand a bendable transformer is also made. It is then applied to an *LLC* converter. Both converters have a power rating of 5 V and 500 mA for a USB power supply. The modeling procedure is described in detail. Both simulation and experimental measurements of a hardware prototype are included to confirm the proposal.

II. Bendable Inductor and Transformer Modeling

A. Analysis by the PEEC Theory

Inductance equations for standard regular shapes have been well documented [24]–[30]. Simple expressions for regular shape inductances are very limited because the flexible winding structure has changeable shapes. A tool for complicated winding structure analysis is needed. A. E. Ruehli proposed the PEEC theory in 1970s [23]. The PEEC theory enables analysis of coupling among interconnections in 3-D multiconductor electronics circuits. This theory states that the effective self-inductance of a winding and mutual inductance of two windings can be calculated by dividing a complex conductor structure into small discrete segments. Integral equations are applied to each elementary piece of the conductor to calculated inductances. Such versatile feature of the PEEC method makes it suitable to calculate self- and mutual inductance of windings with complicated structures, including nonstandard winding structures for wireless power transfer systems.

Mutual inductance between each segment can be calculated by Neumann's formula (1) where l and l' are segments of the primary and secondary conductors. The effective mutual inductance of the elementary elements is

$$L = \frac{\mu}{4\pi}\int_{l}\int_{l'}\frac{dl\cdot dl'}{|r-r'|} \tag{1}$$

The self-inductance of a winding can be calculated similar to the effective mutual inductance as the winding is broken into small discrete segments. However, when integrating the same segment itself, the distance between itself vanishes to zero and results in infinity. Therefore, Rosa's equation for self-inductance of a typical wire for rectangular cross section is used when integrating the same segment [31]. The effective self-inductance of the elementary elements is

$$L = 2l\left[\log\left(\frac{2l}{\alpha+\beta}\right)+0.5+\frac{0.2235\,(\alpha+\beta)}{l}\right](10^{-6}) \tag{2}$$

where l is the length of the straight segment, α is the width, and β is the thickness.

B. Bendable Inductor and Transformer Model

A mathematical model for bendable inductor and transformer is established. Actually both are based on the same principle. An inductor is presented by a single winding and a transformer is presented by grouping two different separate windings at a specified location. Here, a winding structure is divided into many small segments. Define a finite set W to represent the winding. Thus, each conductor segment of the winding is an element of W. Each segment is considered as a straight conductor and represented by a matrix with segment-current vector $\vec{C}_s$ and position vector $\vec{P}_s$. The segment-current vector describes the conductor length and the current direction. The segment-position vector describes the conductor position. Such that

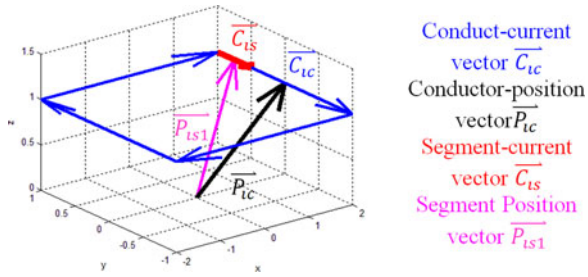

Fig. 1. Single turn coil in three dimension.

$$\mathbf{W} = \left\{w : w \in \left[\vec{C}_s\vec{P}_s\right]\right\} \tag{3}$$

Here, a straight wire is divided in to N segments, the set W has N elements, such that

$$\mathbf{W} = \{w_1, w_2, ..., w_N\}\,\forall w_i \in \left[\vec{C}_s\vec{P}_s\right] \tag{4}$$

$$\mathbf{W} = \{[\vec{C}_{s1}\vec{P}_{s1}], [\vec{C}_{s2}\vec{P}_{s2}], \ldots, [\vec{C}_{sN}\vec{P}_{sN}]\} \tag{5}$$

Fig. 1 shows a single turn rectangular winding on an *xy* plane in three dimensions. Define set $\mathbf{W}_{\mathrm{rect1}}$ to be the rectangular winding and C to be each straight conductor in Fig. 1, such that

$$\mathbf{W_{rect1}} = \mathbf{C_1}\cup\mathbf{C_2}\cup\mathbf{C_3}\cup\mathbf{C_4} \tag{6}$$

Each set $\mathbf{C}_{\mathrm{i}}$ has a conductor-current vector $\vec{C}_{ic}$ and a conductor-position vector $\vec{P}_{ic}$, such that

$$\mathbf{C_i} = \left\{\left[\vec{C}_{ic}\vec{P}_{ic}\right] : \left[\vec{C}_{ic}\vec{P}_{ic}\right] \in \left[\vec{C}_s\vec{P}_s\right]\right\} \tag{7}$$

Each side of the rectangle winding is divided into N segments. The segment-current vectors in a straight conductor are the same because they all lie in the same straight line. However, they have different positions. Such that

$$\mathbf{C_i} = \left\{\left[\vec{C}_{ic}\vec{P}_{ic}\right]\right\} = \left\{\left[\vec{C}_{is}\vec{P}_{is1}\right], \left[\vec{C}_{is}\vec{P}_{is2}\right], \ldots, \left[\vec{C}_{is}\vec{P}_{isN}\right]\right\} \tag{8}$$

where the segment-current vector is

$$\vec{C}_{is} = \frac{\vec{C}_{ic}}{N_i} \tag{9}$$

N_i is the number of segments of $\mathbf{C}_{\mathrm{i}}$ and the segment-position vector is

$$\vec{P}_{isj} = \vec{P}_{ic} - \frac{\vec{C}_{ic}}{2} + \frac{(2i-1)}{2} + \vec{C}_{is} \tag{10}$$

where $i = 1, 2, \ldots, N_i$.

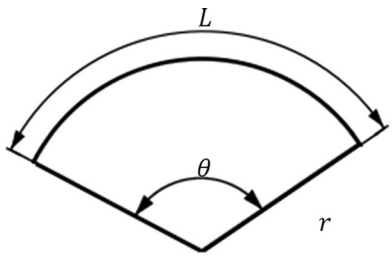

Fig. 2. Bending coil at the side view.

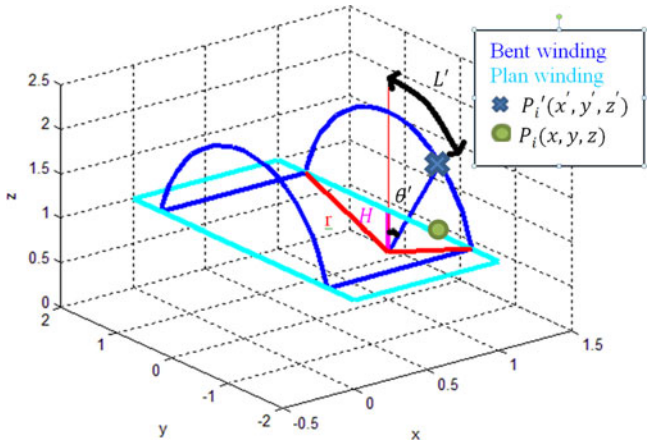

Fig. 3. Geometry of a bending conductor.

The mathematical model of the rectangle winding in Fig. 1 is established by compounding (5)–(7). The total segments number N_{total} is equal to $N_1 + N_2 + N_3 + N_4$. The rectangle winding in Fig. 1 is mathematically represented as

$$\begin{aligned}\mathbf{W_{rect1}} &= \left\{\left[\vec{C}_{s1}\vec{P}_{s1}\right], \left[\vec{C}_{s2}\vec{P}_{s2}\right], \ldots, \left[\vec{C}_{sN}\vec{P}_{sN_{\text{total}}}\right]\right\} \\ &= \left\{\left[\vec{C}_{1c}\vec{P}_{1c}\right], \left[\vec{C}_{2c}\vec{P}_{2c}\right], \left[\vec{C}_{3c}\vec{P}_{3c}\right], \left[\vec{C}_{4c}\vec{P}_{4c}\right]\right\} \end{aligned} \tag{11}$$

$$\mathbf{W_{rect1}} = \left\{\begin{array}{l} \left[\vec{C}_{1s}\vec{P}_{1s1}\right], \left[\vec{C}_{1s}\vec{P}_{1s2}\right], \ldots, \left[\vec{C}_{1s}\vec{P}_{1sN1}\right] \\ \left[\vec{C}_{2s}\vec{P}_{2s1}\right], \left[\vec{C}_{2s}\vec{P}_{2s2}\right], \ldots, \left[\vec{C}_{2s}\vec{P}_{2sN2}\right] \\ \left[\vec{C}_{3s}\vec{P}_{3s1}\right], \left[\vec{C}_{3s}\vec{P}_{3s2}\right], \ldots, \left[\vec{C}_{3s}\vec{P}_{3sN3}\right] \\ \left[\vec{C}_{4s}\vec{P}_{4s1}\right], \left[\vec{C}_{4s}\vec{P}_{4s2}\right], \ldots, \left[\vec{C}_{4s}\vec{P}_{4sN4}\right] \end{array}\right\} \tag{12}$$

Although the flat structure of the winding can be presented by the proposed model easily, a model suitable for a bent structure is not readily available. The segment-current vectors and segment-position vectors may change according to curvature of the bent winding. A method for developing a bendable transformer model is now explained.

Fig. 2 shows a side view of a bent winding. The bending of the winding is described by an arc of a circle. It should be noted

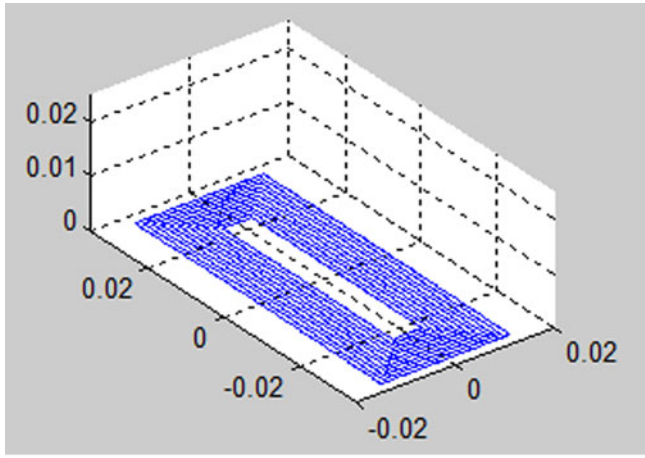

(a)

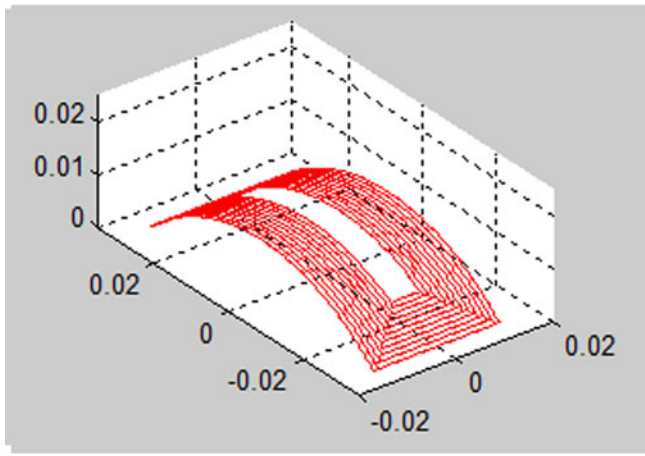

(b)

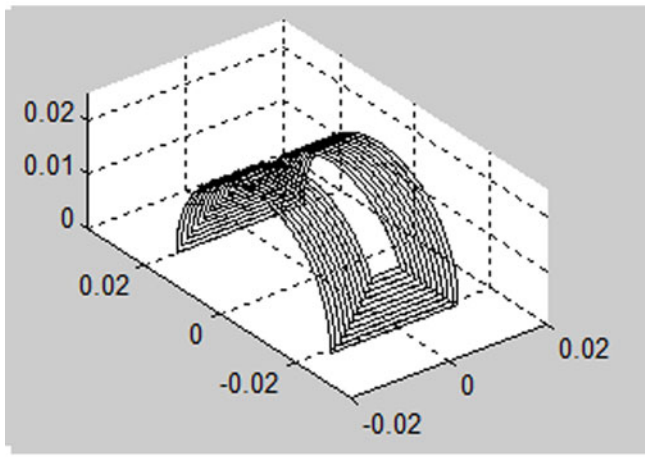

(c)

Fig. 4. Coil bending at different angles. (a) Coil central angle = 0. (b) Coil central angle = $\pi/2$. (c) Coil central angle = π.

that the method applies to any curved geometry in principle. Usually, the arc is described by its central angle and radius. When a winding is bent, the winding length is fixed and equal to the arc length *L*. Angle θ defines the bending and radius r is equal to L/θ. When the bending is increased, the central angle increases and radius decreases. Fig. 4(a) shows the winding at

central angle equals to 0 (i.e., the winding is flat). Fig. 4(b) shows the winding bent with a central angle equals to $\pi/2$ and Fig. 4(c) shows the winding bent with a central angle π.

There are three steps to convert a flat winding model to a bent winding model with reference to Fig. 3. First, convert each segment of the flat winding into a starting point $\vec{S}_{\rm start}$ and an ending point $\vec{S}_{\rm end}$, such that

$$\vec{S}_{\rm start} = \vec{S}_p - \frac{\vec{S}_c}{2} = P_{\rm start}(x,y,z) \tag{13}$$

$$\vec{S}_{\rm end} = \vec{S}_p + \frac{\vec{S}_c}{2} = P_{\rm end}(x,y,z) \tag{14}$$

Second, convert each point of the segments from a flat surface to a curved surface. Define point $P_i(x,y,z)$ as a point on the flat surface and point $P_i'(x',y',z')$ as the same point after bending the transformer structure. When the wire is bent in a plane along the x-axis, the new x-coordinate of each point remains unchanged. The distance between each point on the plane remains unchanged after the transformer is bent. Such that the arc length L' at point P_i' is equal to the *y*-coordinate of point $P_i(x,y,z)$ in Fig. 3. Arc length L is equal to the length of the winding at *x*-axis. Angle θ is equal to the bending angle. The transformation functions from point $P_i(x,y,z)$ to point $P_i'(x',y',z')$ are

$$x' = x \tag{15}$$

$$y' = r\sin(\theta') = r\sin\left(\frac{y}{r}\right) \tag{16}$$

$$z' = z + r\cos(\theta') - H = z + r\cos\left(\frac{y}{r}\right) - r\cos\left(\frac{\theta}{2}\right) \tag{17}$$

where H is the vertical displacement between the original plane and circle center.

Third, create the winding segments of the bent transformer from the new points produced in the second step. The segments of the bent winding model become

$$\vec{S}_c' = \vec{S}_{\rm end}' - \vec{S}_{\rm start}' \tag{18}$$

$$\vec{S}_p' = \frac{\vec{S}_{\rm end}' - \vec{S}_{\rm start}'}{2} \tag{19}$$

In order to establish the mathematical model of the bent winding in Fig. 3, these steps are applied to the model of the same winding before bending. Define the set $\mathrm{W}_{\rm Frect}$ as the flat winding and $\mathbf{W}_{\rm Brect}$ as the bent winding in Fig. 3 such that

$$\mathbf{W_{Frect}} = \left\{ \left[\vec{C}_{s1}\vec{P}_{s1}\right], \left[\vec{C}_{s2}\vec{P}_{s2}\right], \ldots, \left[\vec{C}_{sN}\vec{P}_{sN}\right] \right\} \tag{20}$$

Step 1:

Apply (7) and (8) to set $\mathbf{W}_{\rm Frect}$, such that

$$\mathbf{W_{Frect.Step1}} = \left\{ \begin{array}{l} [P_{\rm start1}(x,y,z)P_{\rm end1}(x,y,z)], \\ [P_{\rm start2}(x,y,z)P_{\rm end2}(x,y,z)], \\ \ldots, \\ [P_{\rm startN}(x,y,z)P_{\rm endN}(x,y,z)] \end{array} \right\} \tag{21}$$

Step 2:

Apply (9), (10) to set $\mathbf{W}_{\rm Frect.Step1}$ to convert the flat winding to bent winding with central angle equals to θ. Arc length L is equal to the length of the winding at *x*-axis

$$\mathbf{W_{Frect.Step2}} = \left\{ \begin{array}{l} [P_{\rm start1}'(x',y',z')P_{\rm end1}'(x',y',z')], \\ [P_{\rm start2}'(x',y',z')P_{\rm end2}'(x',y',z')], \\ \ldots, \\ [P_{\rm startN}'(x',y',z')P_{\rm endN}'(x',y',z')] \end{array} \right\} \tag{22}$$

Step 3:

Apply (11) and (12) to set $\mathbf{W}_{\rm Frect.Step3}$, such that bent winding set $\mathbf{W}_{\rm Brect}$ is

$$\begin{aligned} \mathbf{W_{Brect}} &= \mathbf{W_{Frect.Step3}} \\ &= \left\{ \left[\vec{C}_{s1}'\vec{P}_{s1}'\right], \left[\vec{C}_{s2}'\vec{P}_{s2}'\right], \ldots, \left[\vec{C}_{sN}'\vec{P}_{sN}'\right] \right\} \end{aligned} \tag{23}$$

C. Calculation of Self-inductance

In the previous section, a mathematical model is established for each winding. A set $\mathbf{W} = \{w : w \in [\vec{C}_s\vec{P}_s]\}$ represents a winding. Set $\mathbf{W_1} = \{[\vec{C}_{1s1}\vec{P}_{1s1}], [\vec{C}_{1s2}\vec{P}_{1s2}], \ldots, [\vec{C}_{1sN1}\vec{P}_{1sN1}]\}$ is the winding of the inductor. The self-inductance of the winding is calculated by applying (1) and (2) to the set $\mathbf{W}_1$, such that

$$L_{\rm self} = \sum_{i=1}^{N1}\sum_{j=1}^{N1} f(i,j) \tag{24}$$

$$f(i,j) = \begin{cases} \dfrac{\vec{C}_{1si}\cdot\vec{C}_{1sj}}{\left|\vec{P}_{1si} - \vec{P}_{1sj}\right|}, & \text{for } i \neq j \\ 2l\left[\begin{array}{l}\log\left(\dfrac{2l}{\alpha+\beta}\right) + 0.5 \\ + \dfrac{0.2235(\alpha+\beta)}{l}\end{array}\right](10^{-6}), & \text{for } i = j \end{cases} \tag{25}$$

where l is the length of the straight segment, α is the width, and β is the thickness.

D. Calculation of Mutual Inductance of Two Windings

Define the set W_1 to be the primary winding and $\mathbf{W_2} = \{[\vec{C}_{2s1}\vec{P}_{2s1}], [\vec{C}_{2s2}\vec{P}_{2s2}], \ldots, [\vec{C}_{2sN2}\vec{P}_{2sN2}]\}$ to be the secondary winding.

The mutual inductance is calculated by applying (1) to the set W_1 and W_2, such that

$$L_{\rm mutual} = \sum_{i=1}^{N1}\sum_{j=1}^{N1} \frac{\vec{C}_{2si}\vec{C}_{2sj}}{\left|\vec{P}_{1si} - \vec{P}_{2sj}\right|} \tag{26}$$

TABLE I
SELF-INDUCTANCE OF THE BENDABLE CORELESS PCB TRANSFORMER/INDUCTOR LIE FLAT

	Calculated	Measured	Error
L1 (16T, 1 layer)	19.23 μH	19.22 μH	−0.052%
L2 (18T, 1 layer)	20.89 μH	20.93 μH	0.19%
L3 (20T, 1 layer)	21.77 μH	21.93 μH	0.73%
L4 (22T, 2 layers, 11 turns per layer)	22.67 μH	22.75 μH	0.35%
L5 (24T, 2 layers, 12 turns per layer)	23.96 μH	23.99 μH	0.13%
L6 (26T, 2 layers, 13 turns per layer)	24.67 μH	24.82 μH	0.31%

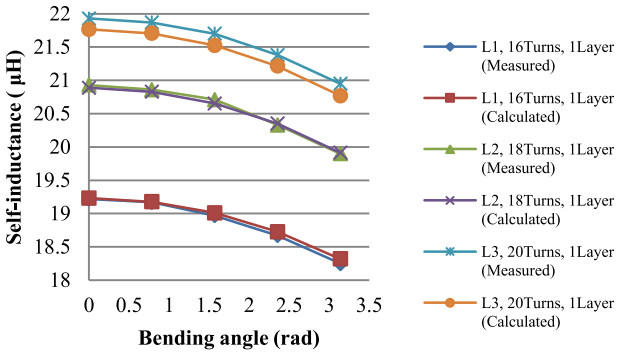

Fig. 5. Self-inductance against bending angle of the first group.

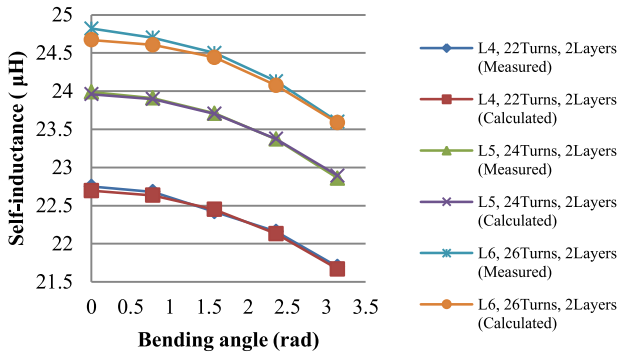

Fig. 6. Self-inductance against bending angle of the second group.

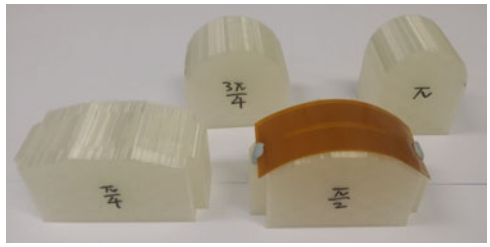

Fig. 7. Support for fixing the bendable angle.

III. BENDABLE INDUCTOR AND TRANSFORMER

Bendable inductors and coreless PCB transformers have been built to verify the mathematical model. The primary and secondary conductors are represented by two segment sets in MATLAB. The inductors are same as the primary side of the transformer. The mutual inductance and self-inductance are calculated by applying the primary and secondary segment sets into (25) and (26). Six inductors and 12 transformers have been built to verify the model. The specifications of the bendable and coreless PCB transformers and inductors are listed in Appendix.

A. Bendable Inductor

There are two groups of inductors. This first group of inductor has winding dimension of 100 mm × 40.25 mm. There are three inductors in this group. The turns number of them are 16, 18, and 20. Inductor L1, L2, and L3 are equal to the primary side of Tx1, Tx2 and Tx3 respectively.

The secondary group of inductor has winding dimensions of 65 mm × 26 mm. There are three inductors in the secondary group. The turns number of them are 22, 24, and 26. Inductor L4, L5, and L6 are equal to the primary side of Tx7, Tx8, and Tx9, respectively.

The calculated and measured self-inductance values of the bendable inductance at flat are shown in Table I. The calculated and measured self-inductance with the bending angle is shown in Figs. 5 and 6. The bending angle of the transformer is fixed by supporters which is printed by the 3-D printer and is shown in Fig. 7. The calculated results are in good agreement with the measurements within a tolerance of 1.5%. Errors mainly arise from manufacturing tolerance. In practice, every segment direction, size, and position have discrepancies between the model and the physical coil. The overall inductance is calculated by integrating all elementary inductances by PEEC theory.

B. Bendable Transformer

There are two groups of transformers. The first group has bigger windings. Transformer Tx1 to Tx6 is the first group with 100 mm × 40.25 mm in dimension. Each transformer has two windings. There are three types of windings in this transformer group: 16 turns each layer, 18 turns each layer, and 20 turns each layer. Transformer Tx1 to Tx3 have the same turns ratio 1:1 but different number of turns. The primary turns to secondary turns ratios of Tx1 is 16:16, Tx2 is 18:18, and Tx3 is 20:20. Transformer Tx4 to Tx6 have different turns ratio. The primary to secondary turns ratio of Tx4 is 16:20, Tx5 is 16:18, and Tx5 is 18:20.

Transformer Tx7 to Tx12 is the second group with small windings. The winding dimensions are 65 mm × 26 mm. There are three types of winding in this transformer group: 22 (2 layers, 11 turns per layer, 0.1 mm gap), 24 (2 layers, 12 turns per layer, 0.1 mm gap), and 26 (2 layers, 13 turns per layer, 0.1 mm gap). Tx7 to Tx9 have the same turns ratio 1:1 but different number of turns. The primary turn to secondary turn of Tx1 is 22:22, Tx2 is 24:24, and Tx3 is 26:26. Transformer Tx10 to Tx12 have different turns ratio. The primary to secondary turns ratio of Tx10 is 22:26, Tx11 is 22:24, and Tx12 is 24:26.

The layout of the transformer Tx10 is shown in Fig. 8. The bendable transformer windings are made of thin copper strips that are printed on a flexible substrate. This method provides the

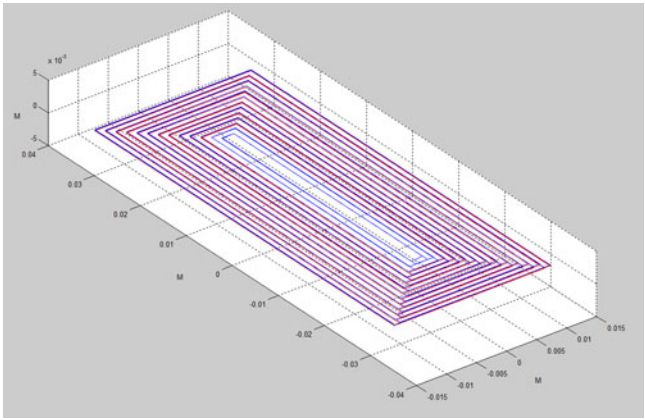

Fig. 8. Layout of the coreless PCB transformer.

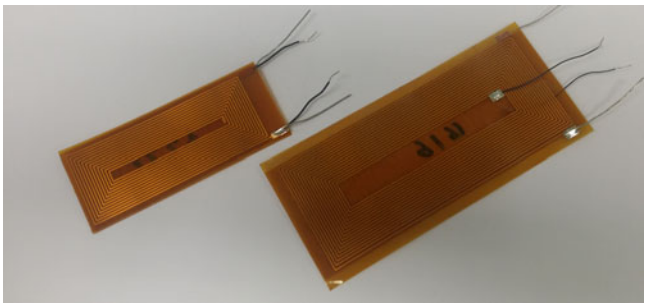

Fig. 9. Bendable transformer prototype.

TABLE II
MUTUAL INDUCTANCE OF THE BENDABLE CORELESS PCB TRANSFORMER LIE FLAT

	Calculated	Measured	Error
Tx1	18.65 μH	18.72 μH	0.38%
Tx2	20.26 μH	20.37 μH	0.54%
Tx3	21.20 μH	21.29 μH	0.42%
Tx4	19.53 μH	19.65 μH	0.61%
Tx5	19.30 μH	19.41 μH	0.57%
Tx6	20.58 μH	20.74 μH	0.78%
Tx7	21.61 μH	21.54 μH	−0.32%
Tx8	22.81 μH	22.84 μH	0.13%
Tx9	23.46 μH	23.63 μH	0.72%
Tx10	22.28 μH	22.33 μH	0.22%
Tx11	22.10 μH	22.10 μH	0%
Tx12	23.06 μH	23.16 μH	0.43%

flexibility for bending the transformer structure. Two prototype are shown in Fig. 9.

The calculated and measured mutual inductance values of the bendable transformer at flat are shown in Table II. The calculated and measured mutual inductance with the bending angle is shown in Figs. 10–13. The calculated agree well with the measurements within a tolerance of 1.5%.

C. Analysis of Bendable Inductor and Transformer

An equivalent transformer model is shown in Fig. 14. The magnetizing inductance, leakage inductance, and equivalent turns ratio are

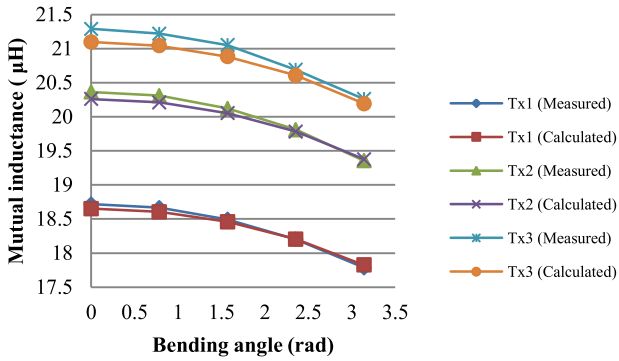

Fig. 10. Mutual inductance of Tx1 to Tx3 (same turns ratio in the first group).

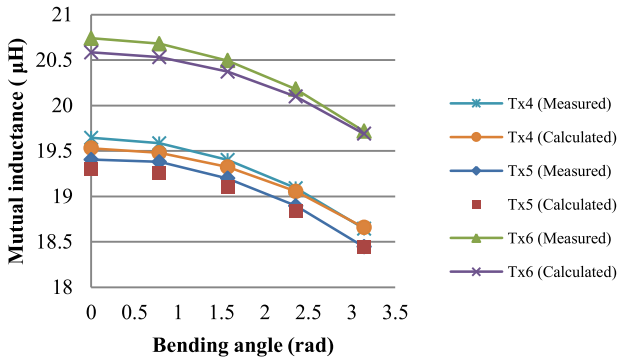

Fig. 11. Mutual inductance of Tx4 to Tx6 (different turns ratio in the first group).

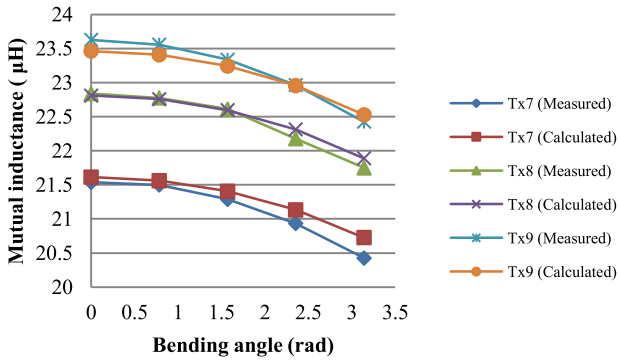

Fig. 12. Mutual inductance of Tx7 to Tx9 (same turns ratio in the second group).

$$K = \frac{L_m}{\sqrt{L_p L_s}} \tag{27}$$

$$L_{\text{mag}} = K^2 L_p \tag{28}$$

$$L_{\text{leak}} = L_p \left(1 - k^2\right) \tag{29}$$

$$\frac{N_p}{N_s} = \frac{L_s}{L_m} \tag{30}$$

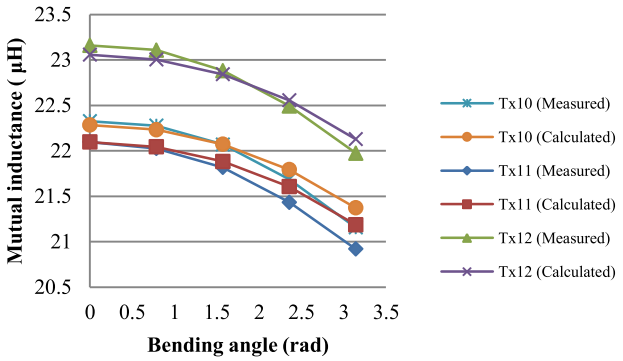

Fig. 13. Mutual inductance of Tx10 to Tx12 (different turns ratio in the second group).

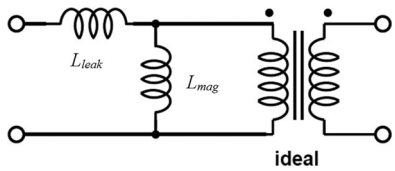

Fig. 14. Equivalent transformer model.

where L_{mag} is the magnetizing inductance, L_{leak} is the leakage inductance, L_p is the primary self-inductance, L_s is the secondary inductance, and K is the magnetic coupling factor.

The variations of the mutual inductance and self-inductance change of the coreless PCB transformer Tx10 versus the bending angle θ are showed in Fig. 15(a) to (c). The equivalent transformer model parameters are shown in Fig. 15(d) and (e).

Fig. 15(a)–(c) shows the variations of the primary self-inductance, secondary self-inductance, and mutual inductance, respectively, with the bending angle. The inductance variations of the inductors and transformers are found to be within 5% of their respective inductance values obtained when the winding is flat. Fig. 15(d) and (e) shows the leakage inductance and magnetizing inductance, respectively. The leakage inductance and magnetizing inductance change could affect resonant frequency in resonant power converter. Fig. 15(f) shows the turns ratio change, which is within 0.5%. The changing of the turns ratio affects the voltage gain in the power converter. These changes should be handled by the feedback controller in the power converter.

IV. Experimental Result on Bendable Converter

Two practical 26–5-V 500-mA (USB 2.0 standard) converters are built to verify the bendable inductor and transformer model. Seven Li polymer batteries each with 3.7 V are used in series as the power source. A buck converter is built with the bendable inductor and an *LLC* resonant converter is built with the bendable transformer. The inductor in the buck converter is used as the primary winding of the transformer in the *LLC* converter for better comparison. Fig. 16 shows the *LLC* resonant converter prototype used in this paper.

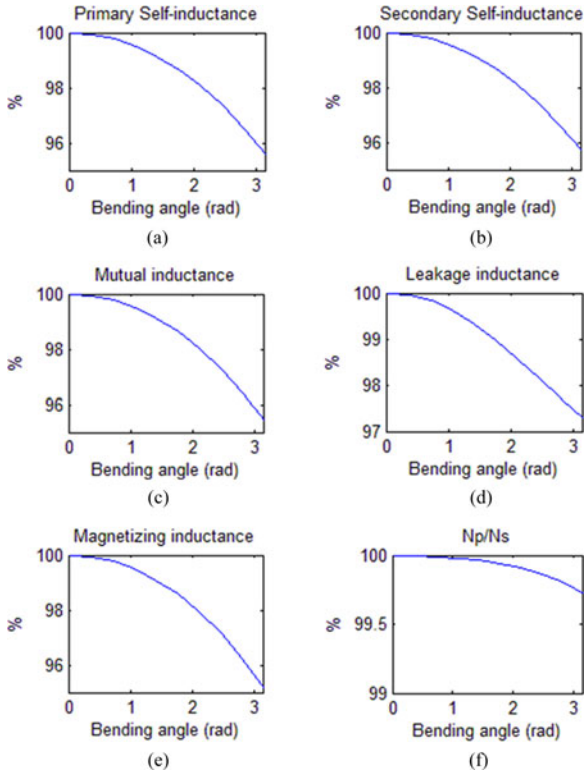

Fig. 15. Inductance against bending angle. (a) Primary self-inductance. (b) Secondary self-inductance. (c) Mutual inductance. (d) Leakage inductane. (e) Magnetizing inductance. (f) Np/Ns.

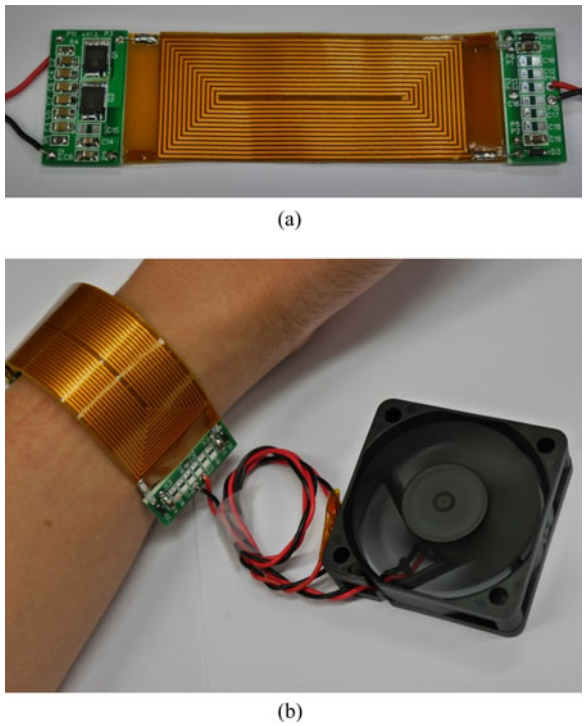

Fig. 16. Bendable transformer prototype. (a) *LLC* converter with bendable transformer. (b) wear the converter which drives a fan.

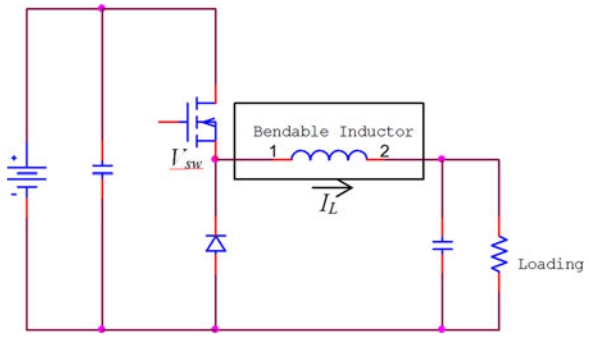

Fig. 17. Simplify buck converter circuit.

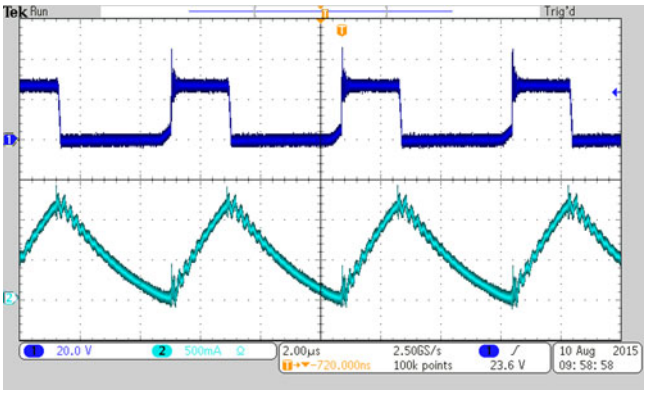

Fig. 18. Buck converter waveforms (Ch1: Switching node; Ch2: Inductor current).

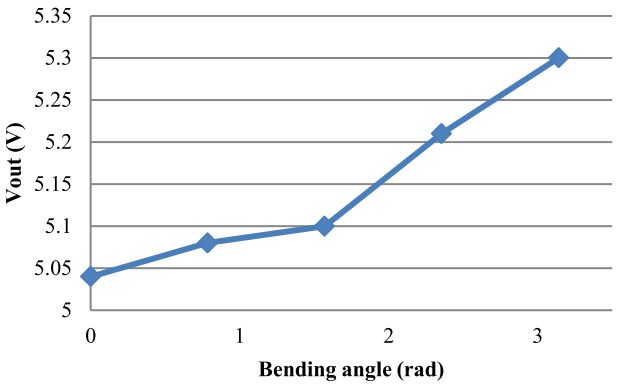

Fig. 19. $V_{\rm out}$ against bending angle (Buck converter).

A. Buck Converter With Bendable Inductor

A buck converter with bendable inductor L4 is built to demonstrate the bendable inductor. The design of the prototype is based on the bendable inductor and transformer model established in this paper. A simplified circuit is shown in Fig. 17. This buck converter is designed to operate at critical mode at full load. The switching frequency of the buck converter is 175 kHz. Fig. 18 shows the waveform of the buck converter. It shows that the buck converter is operating at critical mode. Fig. 19 shows the output voltage of the buck converter against the different bending angle at fixed duty cycle. The output voltage increases by 6% at bending angle equal to π.

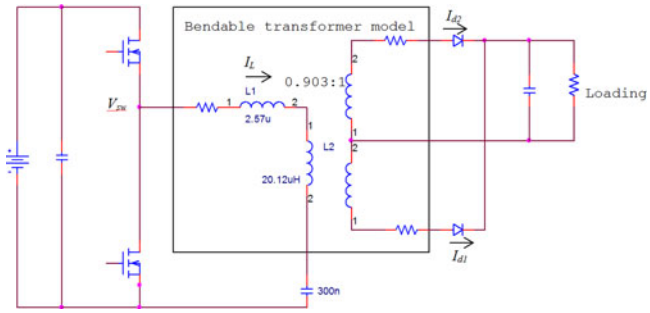

Fig. 20. Simplify *LLC* Converter circuit.

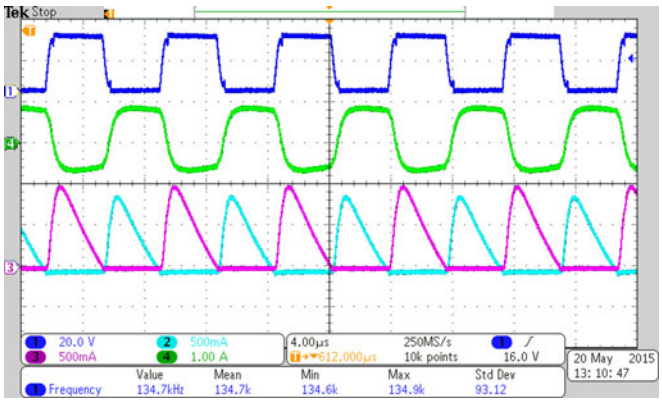

Fig. 21. Prototype waveforms at flat (Ch1: $V_{\rm Sw}$, Ch2: I_{d2}, Ch3: I_{d1}, Ch4: I_L).

B. LLC Resonant Converter With Bendable Transformer

An *LLC* converter is built to verify the bendable transformer model. Nonresonant converter topology usually requires high switching frequency for transformer with low magnetizing inductance. Also, the leakage inductance has to be minimized for high performance. However, bendable transformer has low magnetizing inductance and high leakage inductance. The *LLC* resonant converter topology can operate at a lower switching frequency with low magnetizing inductance transformer. Also, the inherent leakage inductance of the bendable transformer is used as the resonant inductance in the *LLC* resonant converter.

The design of the prototype is based on the bendable transformer model established in this paper. A simplified circuit with equivalent bendable transformer model is shown in Fig. 20. Fig. 21 shows the measured waveforms of the prototype and Fig. 22 shows the simulation waveforms. $V_{\rm Sw}$ is the voltage input of the resonant tank. $V_{\rm Sw}$ shows the switching frequency of the converter. IL is the primary resonant tank current. Figs. 21 and 22 show that the experimental results match well with the simulation.

Fig. 23 shows the measured waveforms of the prototype with bending angle equals to π at the same switching frequency. The calculated resonant frequency of the prototype is 134 kHz at the

Fig. 22. Simulation waveforms (Top: V_{Sw}; Middle: IL, Bottom: Id1, Id2).

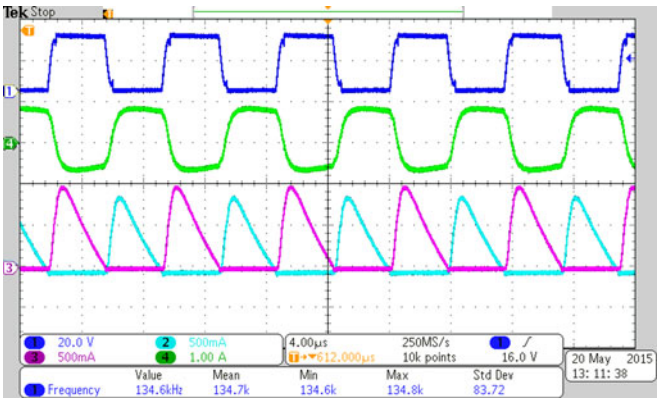

Fig. 23. Prototype waveforms when bent (Ch1: V_{Sw}, Ch2: I_{d2}, Ch3: I_{d1}, Ch4: I_L).

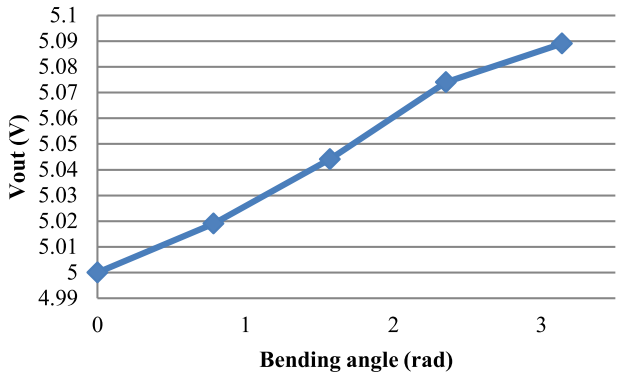

Fig. 24. V_{out} against bending angle at fixed frequency (*LLC* converter).

flat and 141 kHz at the bending angle equal to π. The resonant frequency drifts by 5% when the transformer is bent. Although this frequency drifted is not obvious in the waveform, the output voltage change is considerable.

Fig. 24 shows the output voltage of the prototype against different bending angles at fixed frequency of 134 kHz. The output voltage increases by 1.78% at bending angle equal to π. The gain of the *LLC* resonant converter is fixed by resonant

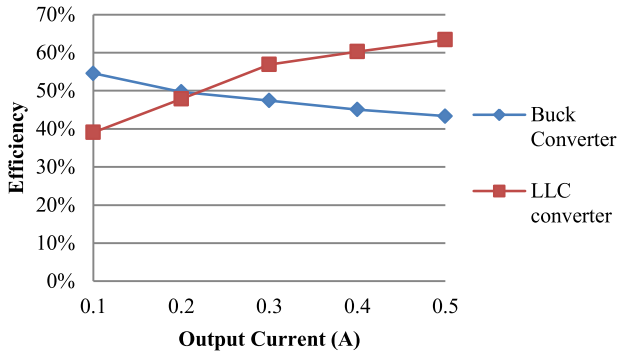

Fig. 25. Efficiency against output current.

tank parameter and switching frequency. In a nonbendable *LLC* resonant converter, the resonant tank parameter is fixed and the output voltage is controlled by the switching frequency. However, the resonant tank parameter of the bendable *LLC* resonant converter changes with the bending angle. This change should be handled by appropriate feedback control in the converter.

C. Buck Converter With Bendable Inductor Versus LLC Converter With Bendable Transformer

Fig. 25 shows the efficiency of the buck converter and *LLC* converter against the loading. For better comparison, the buck converter inductor has the same inductance as the primary winding in the *LLC* converter. The energy efficiency of the buck converter at 26 V input and the output of 5 V and 500 mA is 43%. The energy efficiency of the *LLC* prototype at the same power rating is 63.4%. The energy loss is mainly caused by losses in the bendable transformer and inductor. The winding traces of the bendable transformer and inductor in the prototypes are very thin. The efficiency of the *LLC* converter increases when the loading is increased. This is because when the load increases, the *LLC* converter frequency decreases to maintain regulation. This moves the operation point closer to the resonant frequency. On the other hand, the buck converter efficiency decreases with load. It shows that conduction loss dominates. However, they have comparable efficiencies and *LLC* converter works better at high load.

V. Conclusion

In this paper, two milestones are established. A model for bendable inductor and transformer model based on PEEC theory is established and bendable buck converter and *LLC* resonant converter are built. The bendable transformer is made by printing thin copper tracks on a flexible substrate. A model is introduced such that the conductor of each winding is represented by a set of segment-current and segment-position vectors. A three-step procedure to turn a flat winding model into a bent model is presented. The bendable transformer model shows that both mutual inductance and self-inductance decrease when the transformer is bent by a reasonable amount. The leakage inductance and magnetizing inductance variation are small in this structure as compared with the flat transformer inductance. Based on

APPENDIX
CORELESS PCB TRANSFORMER SPECIFICATIONS

First Group Transformer (same turns ratio):	Tx1	Tx2	Tx3
Primary turns:	16T, 1 layer (L1)	18T, 1 layer (L2)	20T, 1 layer (L3)
Secondary turns:	16T, 1 layer	18T, 1 layer	20T, 1 layer
Primary outer rectangle dimension:		100 mm × 40.25 mm	
Secondary outer rectangle dimension:		100 mm × 40.25 mm	
Conductor cross section dimension:		0.5 mm × 0.01735 mm (0.5 oz)	
Distance between conductors		0.5 mm	
Distance between primary and secondary layer:		0.1 mm	
First Group Transformer (different turns ratio):	Tx4	Tx5	Tx6
Primary turns:	16T. 1 layer	16T, 1 layer	18T, 1 layer
Secondary turns:	20T, 1 layer	18T, 1 layer	20T, 1 layer
Primary outer rectangle dimension:		100 mm × 40.25 mm	
Secondary outer rectangle dimension:		100 mm × 40.25 mm	
Conductor cross section dimension:		0.5 mm × 0.01735 mm (0.5 oz)	
Distance between conductors		0.5 mm	
Distance between primary and secondary layer:		0.1 mm	
Second Group Transformer (2 layer, same turns ratio):	Tx7	Tx8	Tx9
Primary turns:	22T, 2 layers, 11 turns per layer (L4)	24T, 2 layers, 12 turns per layer (L5)	26 (2 layers, 13 turns per layer)
Secondary turns:	22T, 2 layers, 11 turns per layer	24T, 2 layers, 12 turns per layer)	26 (2 layers, 13 turns per layer)
Primary outer rectangle dimension:		65 mm × 26 mm	
Secondary outer rectangle dimension:		65 mm × 26 mm	
Conductor cross section dimension:		5 mm × 0.01735 mm (0.5 oz)	
Distance between conductors		0.5 mm	
Distance between primary and secondary layer:		0.1 mm	
Second Group Transformer (2 layer, different turns ratio):	Tx10	Tx11	Tx12
Primary turns:	22 (2 layers, 11 turns per layer)	22T, 2 layers, 11 turns per layer (L6)	24T, 2 layers, 12 turns per layer
Secondary turns:	26 (2 layers, 12 turns per layer)	24T, 2 layers, 13 turns per layer	26T, 2 layers, 16 turns per layer
Primary outer rectangle dimension:		65 mm × 26 mm	
Secondary outer rectangle dimension:		65 mm × 26 mm	
Conductor cross section dimension:		5 mm × 0.01735 mm (0.5 oz)	
Distance between conductors		0.5 mm	
Distance between primary and secondary layer:		0.1 mm	

the inductor and bendable transformer model, a buck converter with bendable inductor and an *LLC* resonant converter with bendable transformer are built successfully. Both converters have the same power rating of 5 V and 500 mA. The investigation shows that the leakage inductances and the magnetizing inductance can be incorporated as part of the resonant circuit. The practical results confirm that a reasonable energy efficiency of 63.4% for *LLC* converter can be achieved for a rated power of 2.5 W.

REFERENCES

[1] J. P. Ashton, "The design of commercial hearing aids," *Radio Eng., J. Brit. Inst.*, vol. 11, no. 2, pp. 51–59, Feb. 1951.

[2] J. T. Smith, B. O'Brien, Y.-K. Lee, E. J. Bawolek, and J. B. Christen, "Application of flexible OLED display technology for electro-optical stimulation and/or silencing of neural activity," *Display Technol. J.*, vol. 10, no. 6, pp. 514–520, Jun. 2014.

[3] J. Oh, K. Lee, T. Hughes, S. Forrest, and K. Sarabandi, "Flexible antenna integrated with an epitaxial lift-off solar cell array for flapping-wing robots," *IEEE Trans. Antennas Propag.*, vol. 62, no. 8, pp. 4356–4361, Aug. 2014.

[4] C.-Y. Peng, T. P. Dhakal, P. Rajbhandari, S. Garner, P. Cimo, S. Lu, and C. R. Westgate, "Flexible CZTS solar cells on flexible corning willow glass substrates," in *Proc. IEEE 40th Photovoltaic Spec. Conf.*, Jun. 8–13, 2014, pp. 0409–0412.

[5] B. M. Kayes, L. Zhang, R. Twist, I.-K. Ding, and G. S. Higashi, "Flexible thin-film tandem solar cells with >30% efficiency," *IEEE J. Photovoltaics*, vol. 4, no. 2, pp. 729–733, Mar. 2014.

[6] S. Yun, S. Park, B. Park, S. K. Park, H. Prahlad, P. Von Guggenberg, and K.-U. Kyung, "Polymer-based flexible visuo-haptic display," *IEEE/ASME Trans. Mechatronics*, vol. 19, no. 4, pp. 1463–1469, Aug. 2014.

[7] C. Jang, K. Kim, and K. C. Choi, "Toward flexible transparent plasma display: Optical characteristics of low-temperature fabricated organic-based display structure," *IEEE Electron Device Lett.*, vol. 33, no. 1, pp. 74–76, Jan. 2012.

[8] J. Hu, "Overview of flexible electronics from ITRI's viewpoint," in *Proc. 28th VLSI Test Symp.*, Apr. 19–22, 2010, pp. 84–84.

[9] F. Wong and J. Lu, "High frequency planar transformer with helical winding structure," in *Proc. IEEE Int. Magn. Conf. Dig. Tech.*, Apr. 9–13, 2000, pp. 438–438.

[10] A. Bouabana and C. Sourkounis, "Design and analysis of a coreless flyback converter with a planar printed-circuit-board transformer," in *Proc. 12th Int. Conf. Optim. Electr. Electron. Equip.*, May 20–22, 2010, pp. 557–563.

[11] J. Zhang, W. G. Hurley, and W. H. Wolfle, "Design of the planar transformer in LLC resonant converters for micro-grid applications," in *Proc. IEEE 5th Int. Symp. Power Electron. Distrib. Gener. Syst.*, Jun. 24–27, 2014, pp. 1–7.

[12] S. Y. Hui, C. H. Shu-Hung, and S.C. Tang, "Coreless printed circuit board (PCB) transformers for power MOSFET/IGBT gate drive circuits," *IEEE Trans. Power Electron.*, vol. 14, no. 3, pp. 422–430, May 1999.

[13] S.C. Tang, S. Y. Hui, and H. S. H. Chung, "Coreless planar printed-circuit-board (PCB) transformers—A fundamental concept for signal and energy transfer," *IEEE Trans. Power Electron.*, vol. 15, no. 5, pp. 931–941, Sep. 2000.

[14] S. Y. R. Hui and S. C. Tang, "Planar printed-circuit-board transformers with effective electromagnetic interference (EMI) shielding," U.S. Patent 6 501 364, Dec. 31, 2002.

[15] S. Y. R. Hui and S. C. Tang, "Method of operating a coreless printed-circuit-board (PCB) transformer," Eur. Patent EP 0935263B, May 26, 2004.

[16] S. C. Tang, S. Y. R. Hui, and H. Chung, "A low-profile low-power converter using coreless PCB transformer with ferrite polymer composite," *IEEE Trans. Power Electron.*, vol. 16, no. 4, pp. 493–498, Jul. 2001.

[17] M. Munzer, W. Ademmer, B. Strzalkowski, and K. T. Kaschani, "Insulated signal transfer in a half bridge driver IC based on coreless transformer technology," in *Proc. 5th Int. Conf. Power Electron. Drive Syst.*, 2003, vol. 1, pp. 93–96.

[18] P. Luniewski and U. Jansen,; "Unsymmetrical gate voltage drive for high power 1200V IGBT4 modules based on coreless transformer technology driver," in *Proc. 13th Power Electron. Motion Control Conf.*, 2008, pp. 88–96.
[19] International Commission on Non-linizing Radition Protection, "Guidelines for limiting exposure to time-varying electric, magnetic and electromagnetic fields (up to 300 GHz)," *Health Phys.*, vol. 99, no. 6, pp 818–836, Dec. 2010
[20] Y. Ruiyang, G. K. Y. Ho, B. M. H. Pong, B. W.-K. Ling, and J. Lam, "Computer-aided design and optimization of high-efficiency LLC series resonant converter," *IEEE Trans. Power Electron.*, vol. 27, no. 7, pp. 3243–3256, Jul. 2012.
[21] I. D. Thenathayalan and P. Joung-Hu, "A novel series-series-parallel resonant converter topology with loosely coupled transformers," in *Proc. IEEE Int. Conf. Ind. Technol.*, Feb. 26–Mar. 1, 2014, pp. 431–435.
[22] G. Spiazzi and S. Buso, "Effect of a split transformer leakage inductance in the LLC converter with integrated magnetics," in *Proc. Brazilian Power Electron. Conf.*, Oct. 27–31, 2013, pp. 135–140.
[23] A. E. Ruehli, "Equivalent circuit models for three-dimensional multiconductor systems," *IEEE Trans. Microw. Theory Tech.*, vol. 22, no. 3, pp. 216–221, Mar. 1974.
[24] F. W. Grover, *Inductance Calculations: Working Formulas and Tables*. New York, NY, USA: Dover, 2004.
[25] W. G. Hurley and M. C. Duffy, "Calculationof self and mutual impedances in planar sandwich inductors," *IEEE Trans. Magn.*, vol. 33, no. 3, pp. 2282–2290, May 1997.
[26] W. G. Hurley, M. C. Duffy, S. O'Reilly, and S. C. O'Mathuna, "Impedance formulas for planar magnetic structures with spiral windings," *IEEE Ind. Electron.*, vol. 46, no. 2, pp. 271–278, Apr. 1999.
[27] S. I. Babic and C. Akyel, "New analytic-numerical solutions for the mutual inductance of two coaxial circular coils with rectangular cross section in air," *IEEE Trans. Magn.*, vol. 42, no. 6, pp. 1661–1669, Jun. 2006.
[28] S. Babic and C. Akyel, "Improvement in calculation of the self- and mutual-inductance of thin-wall solenoids and disk coils," *IEEE Trans. Magn.*, vol. 36, no. 4, pp. 1970–1975, Jul. 2000.
[29] G. Hurley, M. Duffy, J. Zhang, I. Lope, B. Kunz, and W. Wolfle, "A unified approach to the calculation of self- and mutual-inductance for coaxial coils in air," *IEEE Trans. Power Electron.*, vol. 30, no. 11, pp. 6155–6162, Nov. 2015.
[30] S. Babic, F. Sirois, C. Akyel, and C. Girardi, "Mutual inductance calculation between circular filaments arbitrarily positioned in space: Alternative to Grover's formula," *IEEE Trans. Magn.*, vol. 46, no. 9, pp. 3591–3600, Sep. 2010.
[31] E. B. Rosa and L. Cohen, "Formulae and Tables for the calculation of mutual and self-inductance," *Bull. Bur. Stand.*, vol. 5, pp. 35–50, 1907.

Godwin Kwun Yuan Ho (S'11) was born in Hong Kong in 1985. He received the B.Eng. degree in electrical engineering and the M.Phil. degree in power electronics from the University of Hong Kong, Pokfulam, Hong Kong, in 2010 and 2013, respectively, where he is currently working toward the Ph.D. degree at the Department of Electrical and Electronic Engineering.

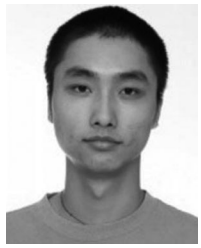

Cheng Zhang (S'13) was born in China in 1990. He received the B.Eng.(first class Hons.) degree in electronic and communication engineering from the City University of Hong Kong, Kowloon, Hong Kong, in 2012. He is currently working toward the Ph.D. degree at the Department of Electrical and Electronic Engineering, University of Hong Kong, Pokfulam, Hong Kong.

His current research interests include designs and optimizations for wireless power transfer applications.

Bryan M. H. Pong (M'84–SM'96) was born in Hong Kong. He received the B.Sc. degree in electronic and electrical engineering from the University of Birmingham, Birmingham, U.K., in 1983, and the Ph.D. degree in power electronics from Cambridge University, Cambridge, U.K., in 1987.

He was a Principal Engineer and Engineering Manager with ASTEC, which is currently Artesyn Embedded Technologies. He is currently an Associate Professor at the Electrical and Electronic Engineering Department, University of Hong Kong, Pokfulam, Hong Kong. He has coinvented a number of patents. His research interests include switching power supply, in particular on synchronous rectification, EMI issues, and design optimization of power converters, planar, and bendable power converters.

S. Y. Ron Hui (F'03) received the Ph.D. degree from Imperial College London, London, U.K., in 1987.

He is currently the Chair Professor of power electronics at the University of Hong Kong (HKU), Pokfulam, Hong Kong, and Imperial College London. At HKU, he holds the Philip Wong Wilson Wong Endowed Professorship in electrical engineering. He has published more than 200 technical papers, including more than 170 refereed journal publications and book chapters and more than 50 of his patents have been adopted by industry.

Dr. Hui is an Associate Editor of the IEEE TRANSACTIONS ON POWER ELECTRONICS and the IEEE TRANSACTIONS ON INDUSTRIAL ELECTRONICS. Since 2013, he has been an Editor of the IEEE JOURNAL OF EMERGING AND SELECTED TOPICS IN POWER ELECTRONICS. He has been appointed twice as an IEEE Distinguished Lecturer by the IEEE Power Electronics Society in 2004 and 2006. He served as one of the 18 Administrative Committee Members of the IEEE Power Electronics Society and was the Chairman of its Constitution and Bylaws Committee from 2002 to 2010. He received the Excellent Teaching Award in 1998. He received an IEEE Best Paper Award from the IEEE IAS Committee on Production and Applications of Light in 2002, and two IEEE Power Electronics Transactions Prize Paper Awards for his publications on Wireless Battery Charging Platform Technology in 2009 and on LED system theory in 2010. His inventions on wireless charging platform technology underpin key dimensions of Qi, the world's first wireless power standard, with freedom of positioning and localized charging features for wireless charging of consumer electronics. In November 2010, he received the IEEE Rudolf Chope R&D Award from the IEEE Industrial Electronics Society, the IET Achievement Medal (The Crompton Medal) and was elected to the Fellowship of the Australian Academy of Technological Sciences and Engineering.